Computationally assisted design of molecularly imprinted polymers for the detection of estrone

Jin Liu
Jilin Agricultural University
Xuhong Cai
Jilin Agricultural University
Junbo Liu
Jilin Agricultural University
Dadong Liang
Jilin Agricultural University
Kaiyin Chen
Jilin Guangxin Engineering Technology Consulting
shanshan tang (tangshanshan81@163.com)
Jilin Agricultural University https://orcid.org/0000-0002-7212-0402
Bao Xu
Jilin Normal University

Research Article

Keywords: estrone, molecularly imprinted polymers, detection, computational design

Posted Date: February 21st, 2022

DOI: https://doi.org/10.21203/rs.3.rs-1356623/v1

Computationally assisted design of molecularly imprinted polymers for the detection of estrone

Jin Liu[1] · Xuhong Cai[1] · Junbo Liu[*,1] · Dadong Liang[1] · Kaiyin Chen[2] · Shanshan Tang[*,1] · Bao Xu[3]

[1]College of Resources and Environment, Key Laboratory of Straw Comprehensive Utilization and Black Soil Conservation, Ministry of Education, Jilin Agricultural University, Changchun 130118, China

[2]Jilin Guangxin Engineering Technology Consulting Co., Ltd, Changchun 130022, China

[3]Institute of Mathematica, Jilin Normal University, Siping, Jilin 136000, China

Abstract Computer simulations are widely used for the selection of conditions for the synthesis of molecularly imprinted polymers and can rapidly reduce the experimental cycle time and save labor and materials. Here, estrone molecularly imprinted polymers (E1-MIPs) were designed at the M062X/6-311+G(*d*,*p*) level with itaconic acid (IA) as the functional monomer. The imprinted molar ratio between E1 and IA was optimized, cross-linkers and solvents were screened, and the nature of interactions between E1 and IA was explored. The simulated results showed that pentaerythritol triacrylate was the best cross-linker and methylbenzene was the best solvent. Meanwhile, when the imprinted molar ratio between E1 and IA was 1:4, the E1-IA complex owned the largest amount of hydrogen bonds, the lowest binding energy, and the strongest stability. The bonding situation of the E1-IA complex was studied using the atoms in molecules analysis. Finally, the study of E1 selectivity using quartz crystal microbalance sensors verified the correctness of theoretical predictions. The computer simulations and experimental studies could provide theoretical guidance for the selection of imprinted molar ratios, cross-linkers, and solvents to synthesize of E1-MIPs. It also could provide important references and directions for the accurate and rapid detection of E1 in water bodies.

Keywords: estrone, molecularly imprinted polymers, detection, computational design

Introduction

Estrone (E1) is an important environmental estrogen that interferes with the reproductive system of aquatic organisms even at extremely low concentrations in environmental water, causing glandular atrophy, functional feminization and altered immune function in males [1]. Not only that, E1 can also harm the human reproductive function through the food chain, inhibit the quantity and quality of sperm, and hinder the growth of egg cells. At the same time, it also has a non-negligible impact on the increase in the incidence of female breast cancer and uterine cancer [2].

Currently, the main detection methods for E1 are gas chromatography [3] and liquid chromatography [4], but in practice, the above detection methods have disadvantages such as long detection cycles, relatively expensive, and require pretreatment. In particular, the C_{18} or C_8 solid-phase extraction packing materials lack specific identification. Thus, it has poor selectivity for the E1.

* Corresponding author: liujb@ccut.edu.cn (Liu JB), tangshanshan@jalu.edu.cn (Tang SS)

Molecular imprinting technology (MIT) refers to the process of preparing molecular imprinted polymers (MIPs) which could match the spatial structure of the template molecule via the polymerization reaction by using the specific target substance (template molecule), suitable functional monomer, cross-linker, and initiator. Compared with the conventional adsorbents used in the pretreatment of the above assays, MIPs have high selectivity, good thermal stability, and high mechanical strength, and also have the advantages of scale preparation, easy operation, and low synthesis cost [5, 6]. Theophylline MIPs were first prepared using a non-covalent method by Mosbach et al [7]. in 1993, which greatly promoted the development of MIT. Now, MIPs are widely used in sensors [8, 9], chromatographic separation [10, 11], and solid phase extraction [12, 13]. With the rapid development of quantum chemistry, more and more researchers are rapidly screening functional monomers, cross-linkers, solvents, and optimal imprinted ratios by computer simulation of MIPs systems [14-16]. For example, the MIPs of hydroxyzine and cetirizine were designed by computer-aided design using the B3LYP method and the selectivity coefficients of potential sensors was predicted based on the simulation results of MIPs [17]. In addition, theoretical calculations can reveal the nature of molecular imprinting and the relationship between structure and properties of complex formed from template molecule and functional monomer. Saied M et al. [18] simulated the geometry of diacetyl platinum (II) complexes at the B3PW91 level and analyzed the chemical bonding nature of complexes using atoms in molecules (AIM) theory.

In the previous studies related to the preparation of E1-MIPs, methacrylic acid (MAA) and acrylamide (AM) were mainly used as functional monomers, ethylene dimethacrylate (EDMA) as cross-linker and methanol as solvent [19, 20]. There are less systematic theoretical studies related to the other novel functional monomers, crosslinkers, and solvents of E1 molecular imprinting systems. Especially, there is nearly no quantitative or semi-quantitative studies on the mechanism and nature of the imprinting action for E1 molecular imprinting systems. Therefore, theoretical and experimental studies of E1 molecular imprinting systems need to be improved. Here, this work investigated the natural bonding orbital (NBO) charges and molecular electrostatic potential (MEP) of E1 and itaconic acid (IA) with the help of DFT to analyze the bonding interaction active sites and screen the optimal interaction ratio, cross-linker, and solvent of the E1-IA imprinting system. The nature of interaction between E1 and IA was explored by the AIM theory. The selectivity of E1 was studied using the quartz crystal microbalance (QCM) sensor.

Computational experimental methods

Materials and instruments

E1, Estriol (E3), diethylstilbestrol (DES), and pentaerythritol triacrylate (PETA) were purchased from Shanghai Aladdin Reagent (Shanghai China). The purities of E1, E3, and DES are over 98%. IA was purchased from Sinopharm Chemical Reagent (Shanghai China). Azobisisobutyronitrile (AIBN) was purchased from Tianjin Guangfu Technology Development (Tianjin China). Tetrahydrofuran, methanol, and acetic, were obtained from Beijing Chemical Works (Beijing China). Polyvinyl Chloride (PVC, 1000 polymerization) was purchased at China Petroleum & Chemical Corporation, Qilu Branch.

Tu-1950 Dual light UV-visible Spectrophotometer was purchased from General Instrument (Beijing China). CHI400C type quartz crystal microbalance analyzer was obtained from Chenhua Instruments (Shanghai China).

Calculation method

In order to select a proper calculation method, the B3LYP, CAM-B3LYP, LC-WPBE, ωB97XD, M062X, and PBEPBE methods with the 6-311+G(*d*,*p*) and 6-31G(*d*,*p*) basis sets were used to optimize the geometry of E1 (Fig. 1). All the calculations were performed with the help of Gaussian 09 program Revision version A.02 software [21].

The bonding sites of E1 and IA were analysed based on the NBO charge and MEP. When the binding energies were calculated, the iterative addition error of the basis functions was corrected using the counterpoise procedure (CP) method proposed by Boys and Bornardi [22]. The single point energy was calculated first, and then the interaction binding energy (ΔE_1) between E1 and IA was calculated using the equation (1).

$$\Delta E_1 = E_C - E_{E1} - \sum E_{IA} \quad (1)$$

E_C is the total energy of the E1-IA stable complex after correction by the CP method. E_{E1} represents the energy of template, and E_{IA} is the sum of energy for monomers.

The binding energy ΔE_2 between E1 (or IA) and cross-linker agent (CA) was calculated using the equation (2):

$$\Delta E_2 = E_C - E_{E1\,or\,IA} - E_{CA} \quad (2)$$

E_C is the total energy of the complex (1:1) formed by E1 (or IA) and cross-linker after correction by CP method. $E_{E1\ or\ IA}$ is the energy of E1 (or IA). E_{CL} is the energy of cross-linker.

Finally, the stable structure of the complex formed when the molar ratio of E1 to IA was 1:1 was placed in the solvent model and the solvation energy (ΔE_3) was calculated using equation (3)

$$\Delta E_3 = E_S - E_V \quad (3)$$

E_S is the interaction energy between E1 and IA in solvent environment. E_V is the interaction energy between E1 and IA under vacuum conditions.

Study on the nature of imprinted polymerization

To reveal the nature of the imprinting action, the charge density, and Laplacian values at the bond critical point (BCP) of the imprinted system was performed based on the atoms in molecules (AIM) theory [23] by using the AIM2000 program.

Preparation of E1-MIPs and NIPs

0.5 mmol (135 mg) E1 and 2 mmol IA were dissolved in 50 mL methanol solvent under ultrasound. 0.1 mol PETA and 0.15 g AIBN were added in the above solution under ultrasound until the powders completely dissolved. The nitrogen was aerated to mixed solution for 5 min. Then the mixed solution was sealed in a water bath at 50 ℃ for 24 h. The resulting polymer was extracted repeatedly with methanol/acetic acid solution (8/2, V/V) using a soxhlet extractor at 70 ℃ until no E1 was detected. The residual acetic acid solution of polymer was removed by extraction with methanol solution for 24 h at 70 ℃. The obtained E1-MIPs was put in the vacuum drying oven at 60 ℃ drying to constant weight. The NIPs were prepared as above except that E1 was not added.

Electrode pretreatment

The QCM electrode surface was washed with piranha solution (30% H_2O_2: 98% H_2SO_4 = 1:3, V/V) for 5 min. Then the QCM electrode was washed with distilled water. The above process was repeated 3~5 times. The QCM electrode was dried with nitrogen and stored in a drying oven for backup.

Construction of molecularly imprinted QCM electrodes

30 mg E1-MIPs, 20 mL tetrahydrofuran, and 20 mg PVC were placed in a 50 mL conical flask under ultrasound for 1 h. The above solution was instilled on the surface of QCM electrode and let stand for 1 h at room temperature to obtain the E1-MIPs modified molecularly imprinted QCM electrode. The NIPs modified QCM electrode was prepared in the same way as described above.

Response characteristics of QCM sensors

The basic principle of the QCM sensor is that when a modified film on the surface of the electrode adsorbs the substrate leading to a change in its weight, the frequency of the quartz crystal substrate will change accordingly. Then it is transmitted to the computer. Using the CHI400 software to analyze and obtain the frequency change signal. The QCM electrode has a reference frequency of 8 MHz and a diameter of 8 mm.

The modified QCM electrode was fixed on the detection cell. 2 mL phosphate buffer (PB, pH = 7) was added to the detection cell as the background solution. The initial frequency (f_0) of the sensor was recorded when the frequency stabilized. Then 10 uL E1 solutions with different concentrations (50, 100, 150, 200, 250, 300 ug/L) was injected into the background solution, respectively. The response frequency (f_i) was recorded after the frequency stabilized. The frequency change (Δf) of the response was calculated according to equation (4).

$$\Delta f = f_i - f_0 \quad (4)$$

The mass absorbed (Δm) of MIPs (NIPs) modified membranes to E1 was calculated using the Sauerbrey equation (5).

$$\Delta m = \frac{\Delta f \cdot A(\rho_q \mu_q)^{1/2}}{-2f^2} \quad (5)$$

f is the reference frequency (Hz); ρ_q is the density (2.648 g/cm^3). μ_q is the shear modulus (2.974×1011 dyn/cm^2). A represents the area (0.205 cm^3).

Study on E1 selectivity

Using E3 and DES as the structural analogs of E1 (Fig. 2), the response values of E1, E3, and DES were measured, respectively, to investigate the selectivity of sensor constructed by E1-MIPs modified QCM electrode. The initial concentrations of E1, E3, and DES standard solutions were 100 ug/L.

Results and discussion

Selection of calculation methods

Table 1 lists the structural parameters of E1 simulated by the six methods (B3LYP, CAM-B3LYP,

WB97XD, M062X, PBEPBE, and ωB97XD) and two basis sets (6-311+G(*d*,*p*) and 6-31G(*d*,*p*)) as well as the experimental data [24]. The data present in Table 1 showed that the structure parameters of E1 calculated by the six methods with two different basis sets were very close, where the deviations of bond lengths were in the range 0.0333 – 0.0338 nm by six methods with the 6-311+G(*d*,*p*) basis set. The deviations of bond angles were in the range 2.3588° - 2.49442°. Compared with the other five methods, the deviation of structural parameters calculated by the M062X method was the smallest, which is closer to the experimental crystal data values. It can also be seen from Table 1 that the bond lengths and bond angles of the two basis sets (6-311+G(*d*,*p*) and 6-31G(*d*,*p*)) under the same method were in the range of 0.0002 - 0.0005 nm and 0.01 - 0.08°, respectively, indicating that the effect of the basis set on the bond lengths and bond angles of the E1 stable structure was small. However, the deviation values of bond length and bond angle (0.0336 nm and 2.3643°) for 6-311+G(*d*,*p*) were smaller compared to those for 6-31G(*d*,*p*) basis set (0.0333 nm and 2.3588°) at the M062X level. Therefore, the M062X/6-311+G(*d*,*p*) method was chosen to optimize the geometric configuration of E1, IA, and E1-IA complexes in this study.

MEP and NBO analysis

According to the calculation results of NBO and MEP, the active sites of E1 and IA will be determined. As can be seen from Fig. 3, the more negative charges were mainly distributed on the O atoms in the carbonyls and hydroxyl group, and the negative charge values were -0.558 (O19) and -0.687 (O20) for E1, respectively. The more positive charges were mainly located on the H atoms in the cyclopentanone, methyl, benzene rings, and hydroxyl groups, and the positive charge values were +0.237 (H21), +0.221 (H32), +0.225 (H33), and +0.471 (H42), respectively. Among them, the charges of O20 and H42 on the hydroxyl group were larger in absolute value. Thus, they were the main dominant active sites of E1. The main active sites of IA were O6 (-0.610), O13 (-0.612), H8 (+0.495), and H15(+0.492), which were O atom in the carbonyls and H atom hydroxyl group.

As seen from the MEP scale in Fig. 3, the electrostatic potential in different regions of the E1 and IA molecules could be shown by different colors. The blue region means the atoms owning more positively charged, and the red region means the atoms owning negatively charged. From Fig. 3(a), one can find that the positive charges of E1 were mostly centered on H21, H32, H33, and H42. The H42 atom on the hydroxyl group had more positively charged and easily got electrons from nucleophile. The negative charges were centered on O19 and O20, which easily lost electrons. Similarly, H8 and H15 on the hydroxyl group in the IA molecule (Fig. 3(b)) could be used as electron acceptors, and O6 and O13 of the carboxyl group could be used as electron donors. The results of MEP analysis were consistent with the results of NBO charge analysis.

Optimization of the molar ratio between E1 and IA

The specific affinity and selectivity of MIPs for substrates relies mainly on the highly ordered steric structure formed by functional monomers in MIPs. This highly ordered steric structure is closely related to the interaction molar ratio between template molecules and functional monomers. The larger the molar ratio between template molecules and functional monomers is, the more ordered the steric structure of the polymer is, and the more stable the conformation is. Thus, it would be promising the synthesis of MIPs with higher affinity, selectivity, and stability. For this reason, the stable conformations of the complexes formed from E1 and IA with different molar ratios (1:1 to 1:4) were

calculated in this study. From Fig. 4 and Table 2, one can find that the amount of hydrogen bonds were 2, 5, 7, and 8, respectively, when the imprinted molar ratios between E1 and IA were 1:1, 1:2, 1:3, and 1:4. The hydrogen bond lengths formed ranged from 0.1706 nm to 0.2563 nm. They were in the range of hydrogen bond [25]. It was obvious that as the molar ratio between E1 and IA increased, the amount of hydrogen bonds also increased gradually. And when the interaction molar ratio of E1-IA reached 1:5, the stable complex could not be formed. Therefore, the optimal molar ratio between E1 and IA was 1:4.

According to Table 2, the binding energies of E1-IA complexes with different molar ratios (1:1, 1:2, 1:3, and 1:4) were -31.73 kJ/mol, -76.24 kJ/mol, -114.52 kJ/mol, and -141.55 kJ/mol, respectively. With the molar ratio between E1 and IA increasing, the binding energy of E1-IA complex decreased, which indicated that the stability of complex formed by template molecule and functional monomer increased. The binding energy was the lowest when the molar ratio between E1 and IA was 1:4, which was expected to form more stable complexes. The results of the binding energy calculations were consistent with the conclusion of the complex stability predicted by the amount of hydrogen bonds in the complex model.

Screening of cross-linker agent

The cross-linking degree of MIPs is influenced not only by the amount of cross-linker, but also by its type. The choice of cross-linker also plays a crucial role in the morphology and mechanical stability of MIPs. To achieve a better imprinting effect, the interaction between the selected cross-linker and IA functional monomer should be greater than that between the cross-linker and E1 when preparing MIPs. So that the polymer could have pores with a defined spatial configuration. And at the same time, the functional residues derived from IA could be ordered in the highly cross-linked E1-MIPs stereospore pores. Fig. 5 showed the binding energy between three CAs (ethylene dimethacrylate, EDMA, pentaerythritol triacrylate PETA, and trimethylolpropane trimethacrylate, TRIM) and E1 (or IA) at a reaction ratio of 1:1. As shown in Fig. 5, the binding energies between the three CAs and E1 were all higher than those and IA, respectively, which indicated that all three CAs were suitable for E1-MIPs. Among them, PETA had the highest binding energy with E1 (-12.16 kJ/mol) and the lowest binding energy with IA (-44.62 kJ/mol), which indicated that PETA had the weakest interaction with E1 and the strongest interaction with IA. Thus, PETA was the most suitable CA for preparation of E1-MIPs.

Selection of solvents

In the synthesis of MIPs, the solvent not only acts as a dispersing medium to disperse all components of the polymerization reaction into a homogeneous phase, but also determines the strength of the non-covalent interaction between the template molecule and functional monomer, the polymer morphology, and the polymer-specific adsorption and selectivity properties. Table 3 shows the solvation energy (ΔE_3) and the C11-H33□O48 hydrogen bond length of the E1-IA stable complex (1:1) in five solvents: water (H_2O), acetonitrile (ACN), methanol (MT), tetrahydrofuran, (THF) and methylbenzene (TL), respectively, which were calculated according to equation (3). The shorter hydrogen bond length and the higher solvation energy meant that the solvent had less influence on the interaction between the E1 and IA. From the data in Table 3, it could be seen that ΔE_3 values of E1-IA stable complex in different solvents was: TL > THF > MT > ACN > H_2O. The larger ΔE_3 value leading to lower polarity of solvent and less interference on interaction between the imprinted molecule and functional monomer, which could significantly improve the specific adsorption and selectivity of MIPs.

Among the above five solvents, TL had the largest ΔE_3 value (-28.33 kJ/mol) and the C11-H33□O48 had the shortest bond length (0.2412 nm) in the E1-IA stable complex. It indicated that TL had the least influence on the interaction between E1 and IA. Thus, it was judged that TL was the preferred solvent for the synthesis of E1-MIPs, followed by THF, MT, ACN, and H_2O.

In the preparation of MIPs, the solvent must be able to dissolve the various reagents required in the polymerization reaction. The solubility and adsorption properties of different reaction components (E1, IA, PETA, and AIBN) in different solvents (H_2O, ACN, MT, THF, and TL) were investigated. The initial concentration of E1 in the experiment was 80 mg/L. As shown in Table 4, all the reaction components were only soluble in ACN and MT, but slightly soluble in other solvents. The theoretical results suggested that TL was the best solvent, however, the reactant components were not soluble in it. It could also be seen from Table 4, the amount of adsorption was greater when MT was used as a solvent. Therefore, MT was chosen as the solvent for the preparation of E1-MIPs in this experimental study. Meanwhile, the solvation energy of MT was greater than that of ACN, further verifying the consistency of theory and experiment.

The nature of imprinting interaction

According to the AIM electron density topological analysis theory proposed by Bader [26], the nature of the interaction between E1 and IA was analyzed. From the molecular diagram of the E1-IA stable complex (1:1) (Fig. 6(a)), one can find that there was a bond critical point (BCP) between O20 on the hydroxyl group in E1 and H50 on the hydroxyl group in IA, and the BCP connected O20 and H50 through two bond paths. Similarly, between H33 on the benzene ring in E1 and O48 on the carbonyl group in IA, and the BCP connects H33 and O48 through two bond paths. It indicates that there was a bonding interaction between E1 and IA. From the Laplacian of the electronic density in Fig. 6(b), it could be seen that in the E1-IA stable complex, the O20 atom of E1 and its point of electron concentration as well as H50 atom of IA and its the point of electron deconcentration were in a line. Similarly, the O48 atom of IA and its point of electron concentration as well as H33 atom of E1 and its point of electron deconcentration were in a line. The calculated results satisfied the geometrical structural features of hydrogen bond formation, which provided evidence for the formation of hydrogen bonds between IA and E1.

In order to quantitatively described the influence of hydrogen bonding characteristics and hydrogen bond formation on the E1-IA stable complex (1:1), their charge density ($\rho(r)_{bcp}$), the Laplacian ($\square^2\rho(r)_{bcp}$), and the energy density of electrons (E_H) of hydrogen bonding at BCP were calculated, respectively. The results were listed in Table 5.

According to reference[26], $\rho(r)_{bcp}$ and $\square^2\rho(r)_{bcp}$ values at BCP could reflect the nature of the chemical bond. The larger the value of $\rho(r)_{bcp}$ at BCP was, the stronger the chemical bond formed. When $\square^2\rho(r)_{bcp}$ value was larger than 0, the chemical bond was a hydrogen bond. In addition, the energy density (V(r)) of electrons also predicts the strength and nature of hydrogen bonds with the energy relationship $E_H = 0.5$ V(r), an-d the hydrogen bond energy should be no less than -42 kJ/mol. As can be seen from Table 5, the $\square^2\rho(r)_{bcp}$ values at BCP between H50□O20 and H33□O48 were 0.1229 and 0.0353 a.u. respectively. It satisfied the requirement of forming hydrogen bond which proposed by Rozas et al [27]. The $\rho(r)$ values at BCP were 0.0304 and 0.0105 a.u., respectively. The $\rho(r)_{bcp}$ values between H50 and O20 were larger than those between H33 and O48, indicating that the strength of hydrogen bonding between the former was larger than that of the latter. It was consistent with the calculated results of hydrogen bond length. In addition, the EH values (-35.58 and -8.27 kJ/mol) of

interaction sites were greater than -42 kJ/mol. All the above calculations indicated that E1 interacts with the IA through hydrogen bonding.

Response characteristics of QCM sensors

The response values of E1-MIPs and NIPs-modified QCM sensors were examined when the E1 standard solutions concentrations are 50, 100, 150, 200, 250 and 300 ug/L, respectively, with the pH value of PB background solution is 7, addition of E1-MIPs is 30 mg, and coating amount of PVC is 20 uL. The corresponding E1 adsorption amounts were calculated and the results are shown in Fig. 7. The sensor response was enhanced as the concentration of the standard solution increased, corresponding to an increase in the amount of E1 adsorbed. Among them, the frequency variation of the E1-MIPs modified QCM sensor was much higher than that of the NIPs modified sensor. And the difference in adsorption effect increased with increasing concentration of the standard solution. The regression equation for the response frequency of the E1 molecularly imprinted QCM sensor over the detection concentration range was Y = -2.6255X-12.685 (R^2 = 0.9983). The minimum line of detection (LOD) could be calculated by the equation LOD = 3.3 δ/S. δ denotes the residual standard deviation of the regression line and S denotes the slope of the regression line. Thus, the LOD value is 16.00 ug/L for the present E1 molecularly imprinted QCM sensor.

Selectivity of QCM sensors

To investigate the selectivity of the E1 molecularly imprinted QCM sensor for E1, the response frequencies of the QCM sensor to E1 and its structural analogs (E3 and DES) were measured, respectively. As can be seen from Fig. 8, the QCM sensor has a certain response to E1, E3, and DES, and the response frequency was in the order of E1 > E3 > DES. Among them, the highest frequency of sensor response to E1 was due to the presence of functional groups complementary to the E1 functional group in E1-MIPs, thus the sensor response to E1 has the highest value. In addition, both E3 and E1 contained the same benzene ring and cyclopentanone ring with the same reactive groups and similar structures, which were relatively better matched with the imprinted holes of E1-MIPs, so the response frequency of E1 molecularly imprinted QCM sensors to E3 was greater than that to DES. The above results indicated that the E1 molecularly imprinted QCM sensor has good selective recognition ability for E1, and also demonstrated the specific adsorption of MIPs.

Conclusion

The M062X/6-311+G(*d*,*p*) method of DFT was used to simulate the bonding sites and spatial configuration of the complexes formed by E1 as the template molecule and IA as the functional monomer, and optimize the imprinting molar ratio, cross-linker agent, and solvent. The nature of the bonding interaction was further investigated by the electron density topology analysis of the complexes formed by E1 and IA. The theoretical results indicated that E1 interacted with IA through hydrogen bonding, and E1-MIPs with higher specific adsorption could be prepared with PETA as the CA with the molar ratio of 1:4. The experimental results show that the E1 molecularly imprinted QCM sensor has a good selective recognition ability, which was consistent with the theoretical study. The LOD of sensor was 16.00 ug/L. This work provides an important reference for achieving accurate and rapid detection of E1 in water bodies and a theoretical reference for the preparation of E1-MIPs. It also provides a

basis for computer simulation to design imprinting systems combine with QCM technology to construct novel sensors.

Declarations

Funding

The Science and Technology Development Planning of Jilin Province (20200201202JC).

Conflict of interest

The authors declare no competing interests.

Availability of data and material

Not applied.

Code availability

Not applied.

Author contribution

Jin Liu: conceptualization, formal analysis, experiment, writing original draft preparation; Shanshan Tang, Junbo Liu, and Dadong Liang: visualization, funding, writing, review, and editing the manuscript; Xuhong Cai: formal analysis and methodology; Kaiyin Chen: test and analysis; Bao Xu: software. All authors have read and agreed to the published version of the manuscript.

References

[1] Patel S, Homaei A, Raju AB (2018) Estrogen: The necessary evil for human health, and ways to tame it. Biomed Pharmacother 102:403-411. https://doi.org/10.1016/j.biopha.2018.03.078

[2] Di NA, Foresta C (2019) Water and soil pollution as determinant of water and food quality/contamination and its impact on male fertility. Reprod Biol Endocrin 17: 4-16. https://doi.org/10.1186/s12958-018-0449-4

[3] Evans RL, Rushing LG, Billedeau SM, Holder CL, Siitonen, PH (2005**)** Trace analysis of ethinyl estradiol in casein diet using gas chromatography with electron capture detection. J Chromatogr Sci 43: 76-80. https://doi.org/10.1093/chromsci/43.2.76

[4] Nelson RE, Grebe SK, Kane DJ, Singh RJ (2004**)** Liquid Chromatography–Tandem Mass Spectrometry Assay for Simultaneous Measurement of Estradiol and Estrone in Human Plasma. Clin Chem 50:373-384. https://doi.org/10.1373/clinchem.2003.025478

[5] Kazım K, Yalçın KD, Lokman U (2021) Molecularly imprinted polymers in toxicology: a literature survey for the last 5 years. Environ Sci Pollut Res Biol 28: 1-35. https://doi.org/10.1007/s11356-021-14510-4

[6] Bashir K, Guo PQ, Chen GN, Li YZ, Ge YH (2020) Synthesis, characterization, and application of griseofulvin surface molecularly imprinted polymers as the selective solid phase extraction sorbent in rat plasma samples. Arab J Chem 13: 4082-4091. https://doi.org/10.1016/j.arabjc.2019.06.007

[7] Vlatakis G, Andersson LI, Müller, R (1993) Drug assay using antibody mimics made by molecular imprinting. Nature 361:645-647. https://doi.org/10.1038/361645a0

[8] Ai J B, Guo H, Xue R, Wang X, Lei X, Yang W (2018) A self-probing, gate-controlled, molecularly imprinted electrochemical sensor for ultrasensitive determination of p -nonylphenol. Electrochem Commun.89: 1-5. https://doi.org/10.1016/j.elecom.2018.02.008

[9] Ozcelikay G, Kurbanoglu S, Zhang XR, Soz CK (2021) Electrochemical MIP Sensor for Butyrylcholinesterase. Polymers-Basel J 11:1970-1980. https://doi.org/10.25932/publishup-50185

[10] Wu Y, Zhang WP, Chen Y, Chen ZL. (2015) Electroosmotic pump-supported molecularly imprinted monolithic column for capillary chromatographic separation of nitrophenol isomers. Electrophoresis. 36: 2881-2887. https://doi.org/10.1002/elps.201500085

[11] Nunez O, Gallart-Ayala H, Martins CPB, Lucci PJ (2011) New trends in fast liquid chromatography for food and environmental analysis. Chromatogr A 1228: 298-323. https://doi.org/10.1016/j.chroma.2011.10.091

[12] Zhu GF, Cheng GH, Wang PY, Li WW, Wang YC, Fan J (2019) Water compatible imprinted polymer prepared in water for selective solid phase extraction and determination of ciprofloxacin in real samples. Talanta A 200: 307-315.https://doi.org/10.1016/j.talanta.2019.03.070

[13] Schneider F, Piletskyk S, Piletska E, Guerreiro A (2010) Comparison of thin-layer and bulk MIPs synthesized by photoinitiated in situ crosslinking polymerization from the same reaction mixtures. Appl Polym Sci 98: 362-372. https://doi.org/10.1002/app.22112

[14] Dai ZQ, Liu JB, Tang SS, Wang Y, Li B, Jin RF (2016) Theoretical design and selectivity researches on the enrofloxacin imprinted polymer. Struct Chem 27:1135-1142. https://doi.org/10.1007/s11224-015-0735-0

[15] Marć M, Kupka T, Wieczorek PP, Namieśnik J (2018) Computational modeling of molecularly imprinted polymers as a green approach to the development of novel analytical sorbents. Trends Environ Anal 98: 64-78. https://doi.org/10.1016/j.trac.2017.10.020

[16] Rohani FG, Mohadesi A, Ansari M (2019) A new diosgenin sensor based on molecularly imprinted polymer of para aminobenzoic acid selected by computer-aided design. J Pharmaceut Biomed 174: 552-560. https://doi.org/10.1016/j.jpba.2019.04.044
[17] Azimi A, Javanbakht M (2014) Computational prediction and experimental selectivity coefficients for hydroxyzine and cetirizine molecularly imprinted polymer based potentiometric sensors. Anal Chim Acta 812:184-190. https://doi.org/10.1016/j.aca.2013.12.042
[18] Soliman, SM, Zaid, MM (2019) Applicability of NBO and AIM Topology Analyses to Chemical Bonding in Some Diacetylplatinum(II) Complexes. Asian J Chem 31: 925-937. https://doi.org/10.14233/ajchem.2019.21806
[19] Wang X, Huang P, Ma X, Du X, Lu X (2018) Enhanced In-Out-Tube Solid-Phase Microextraction by Molecularly Imprinted Polymers-Coated Capillary followed by HPLC for Endocrine Disrupting Chemicals Analysis. Talanta 194: 7-13. https://doi.org/10.1016/j.talanta.2018.10.027
[20] Wang S, Xu ZX, Fang GZ, Zhang Y, He JX (2015) Separation and determination of estrone in environmental and drinking water using molecularly imprinted solid phase extraction coupled with HPLC. J Sep Sci 31: 1181-1188. https://doi.org/10.1002/jssc.200700575
[21] Frisch MJ, Trucks GW, Schlegel HB, Scuseria GE, Robb MA, Cheeseman JR, Scalmani G, Barone V, Mennucci B, Petersson GA (2009) Gaussian 09. Revision A.02, Gaussian Inc, Pittsburgh PA.
[22] Aqababa H, Tabandeh M, Tabatabaei M, Hasheminej M (2013) Computer-assisted design and synthesis of a highly selective smart adsorbent for extraction of clonazepam from human serum. Mat Sci Eng C-Mater 33: 189-195. https://doi.org/10.1016/j.msec. 2012.08.029
[23] Bader RF (1994) Atoms in Molecules: A Quantum Theory. Oxford , UK
[24] Zhurova E A, Matta CF, Wu N, Zhurov VV, Pinkerton AA (2006) Experimental and Theoretical Electron Density Study of Estrone. J Am Chem Soc 128: 8849-8861. https://doi.org/10.1021/ja061080v
[25] Zhang BC, Fan X, Zhao DY (2018) Computer-Aided Design of Molecularly Imprinted Polymers for Simultaneous Detection of Clenbuterol and Its Metabolites. Polymers-Basel 11: 17-37. https://doi.org/10.3390/polym11010017
[26] Bader RFW (1991) A quantum theory of molecular structure and its applications. Chem Rev 91: 893-928. https://doi.org/10.1021/cr00005a013
[27] Rozas I, Alkorta I, Elguero J (1997) Field effects on dihydrogen bonded systems. Phys Chem A 275: 423-428. https://doi.org/10.1016/S0009-2614(97)00767-7

Figures

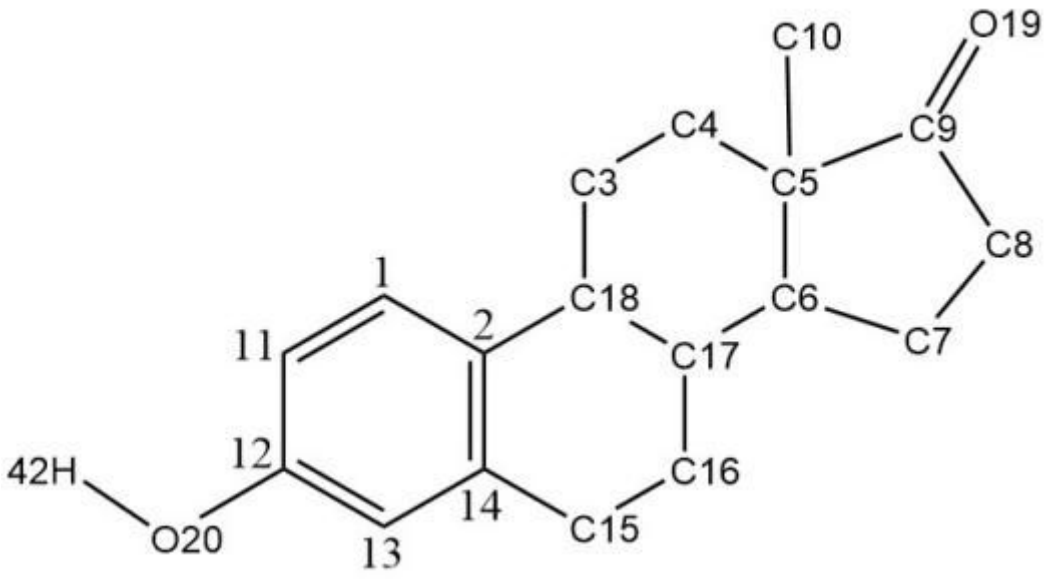

Figure 1

The molecular structure of E1

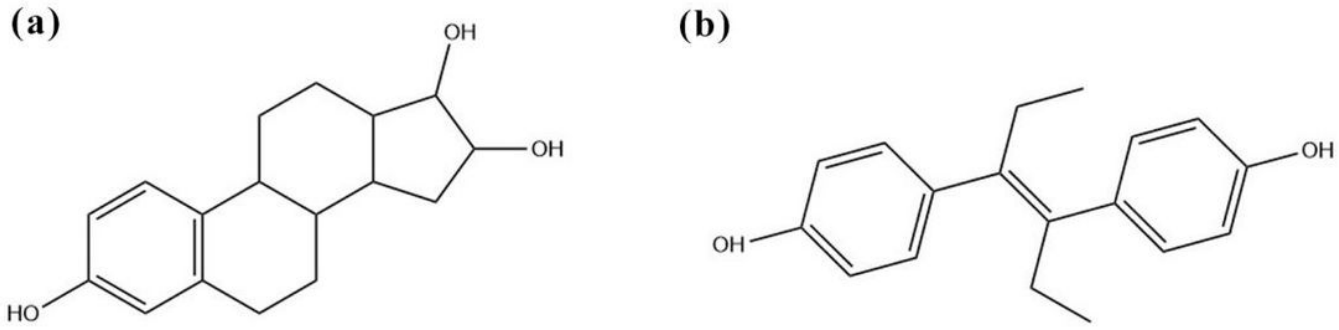

Figure 2

Molecular structure of E3 (a) and DES (b).

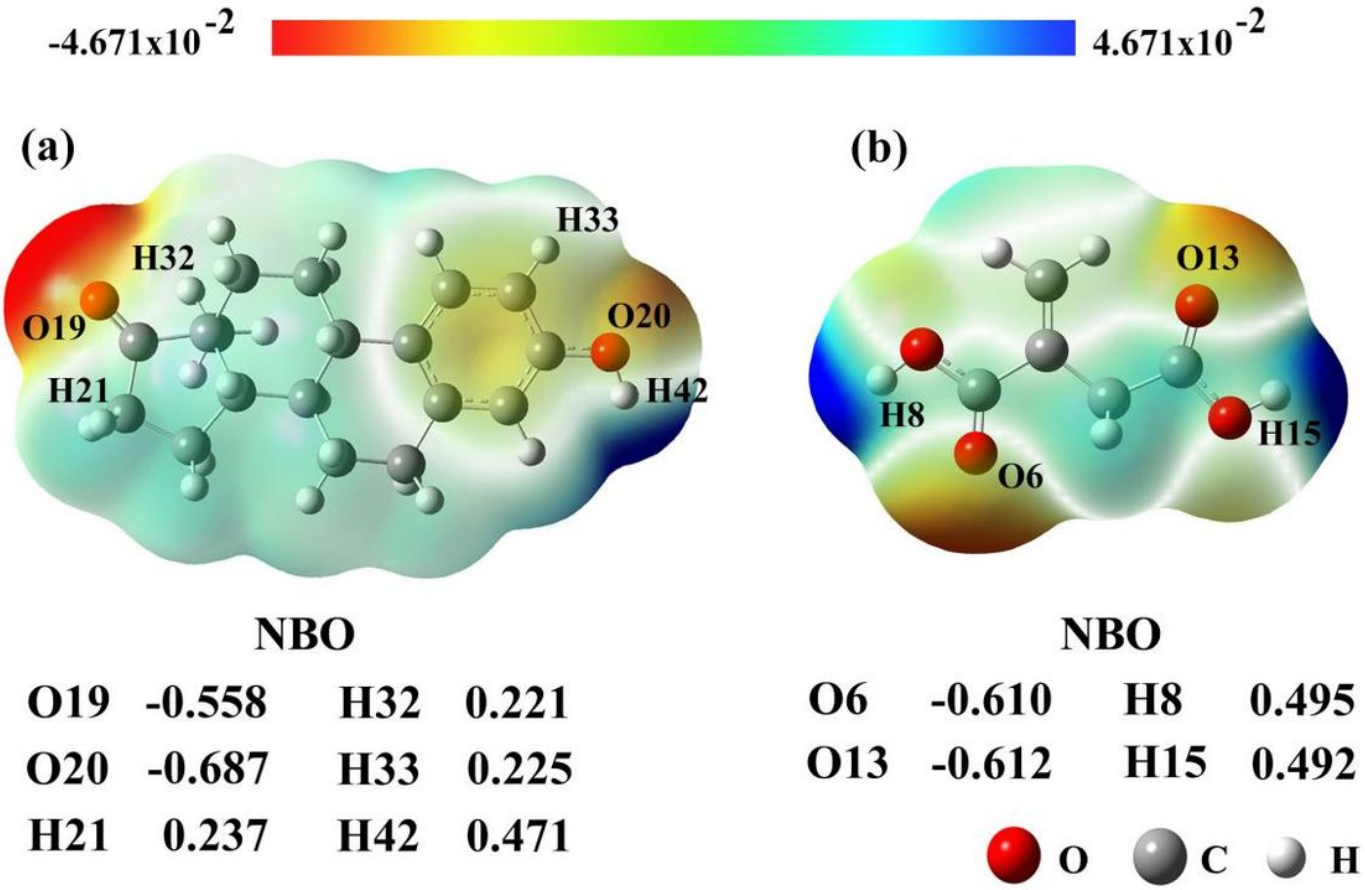

Figure 3

MEP distributions and NBO charges of E1 (a) and IA (b)

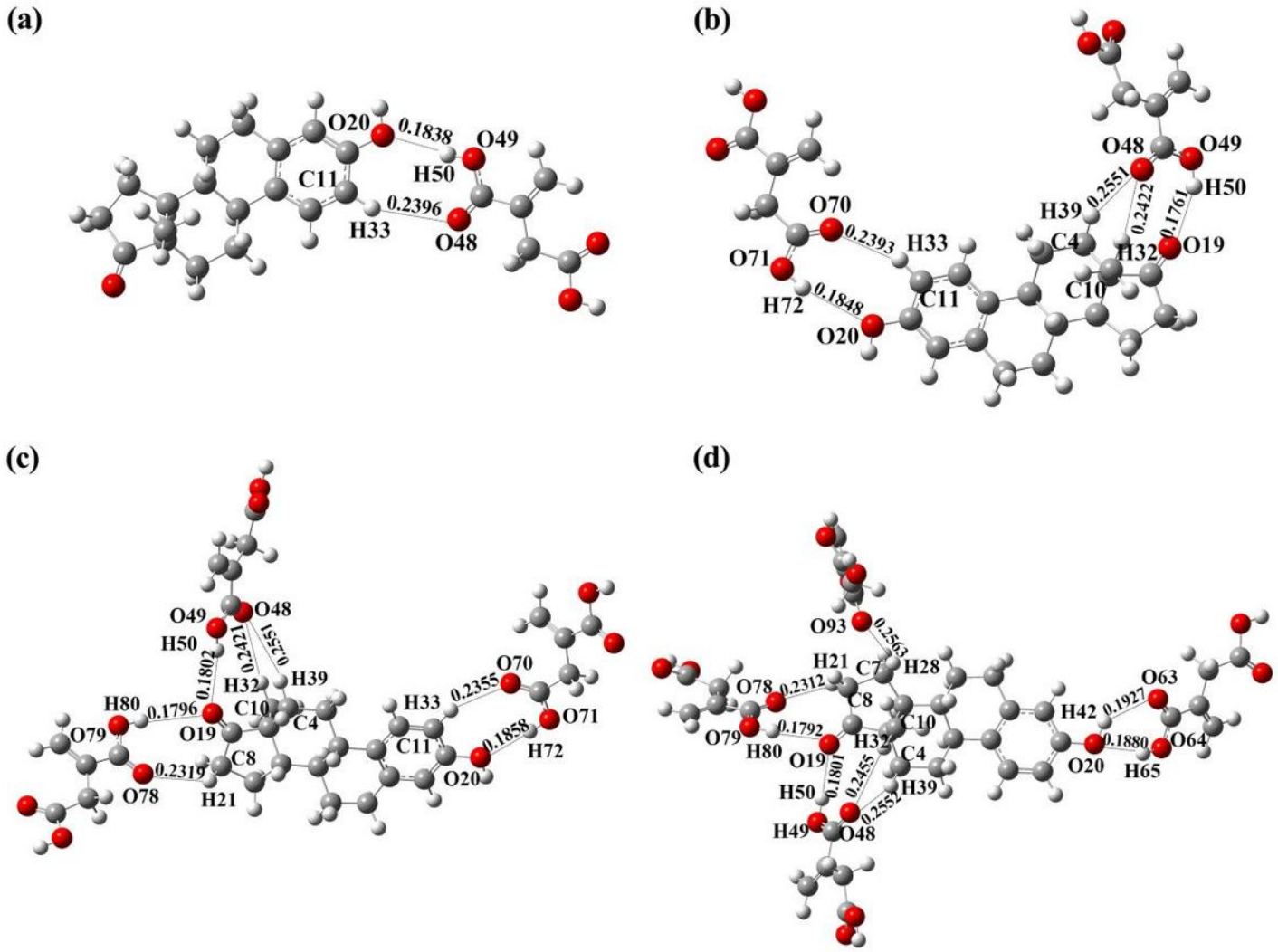

Figure 4

Complexes formed from E1 and IA with different imprinted ratios: (a)1:1, (b)1:2, (c)1:3, and (d)1:4

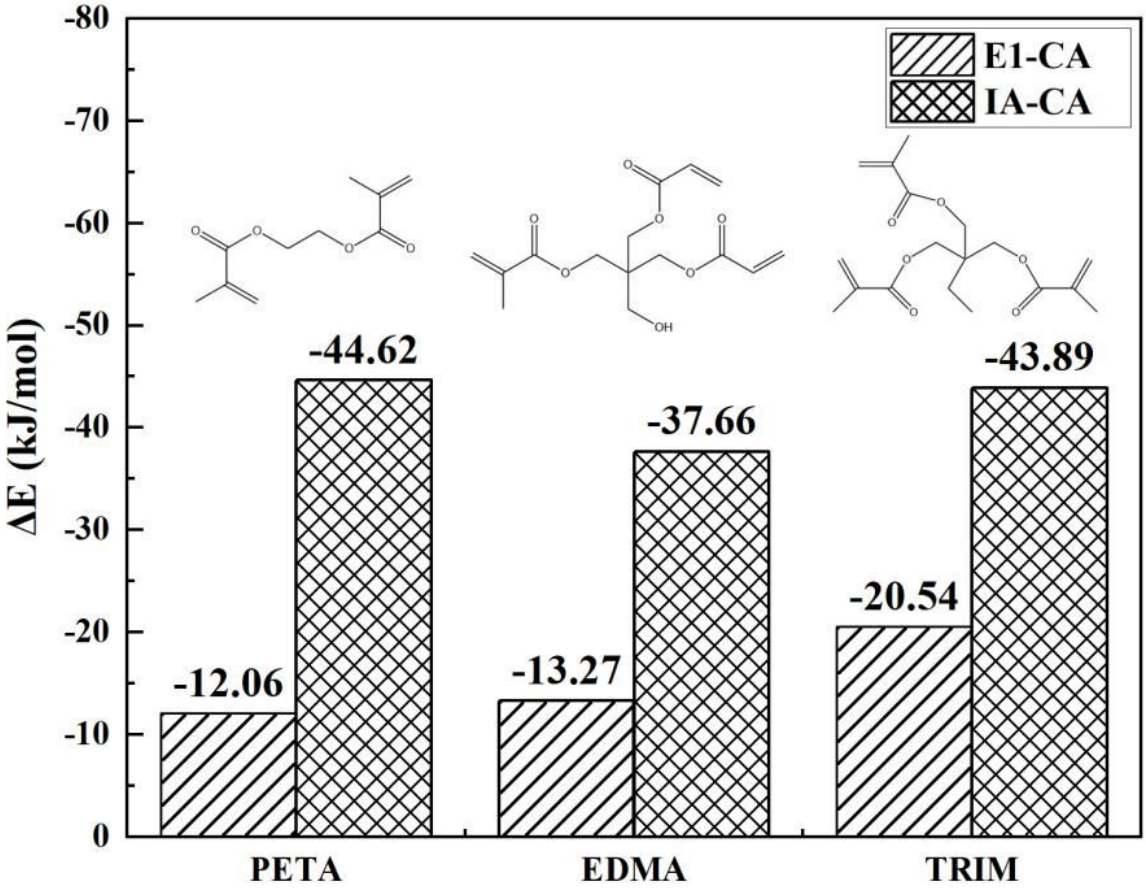

Figure 5

ΔE_2 values between E1 and CA as well as IA and CA

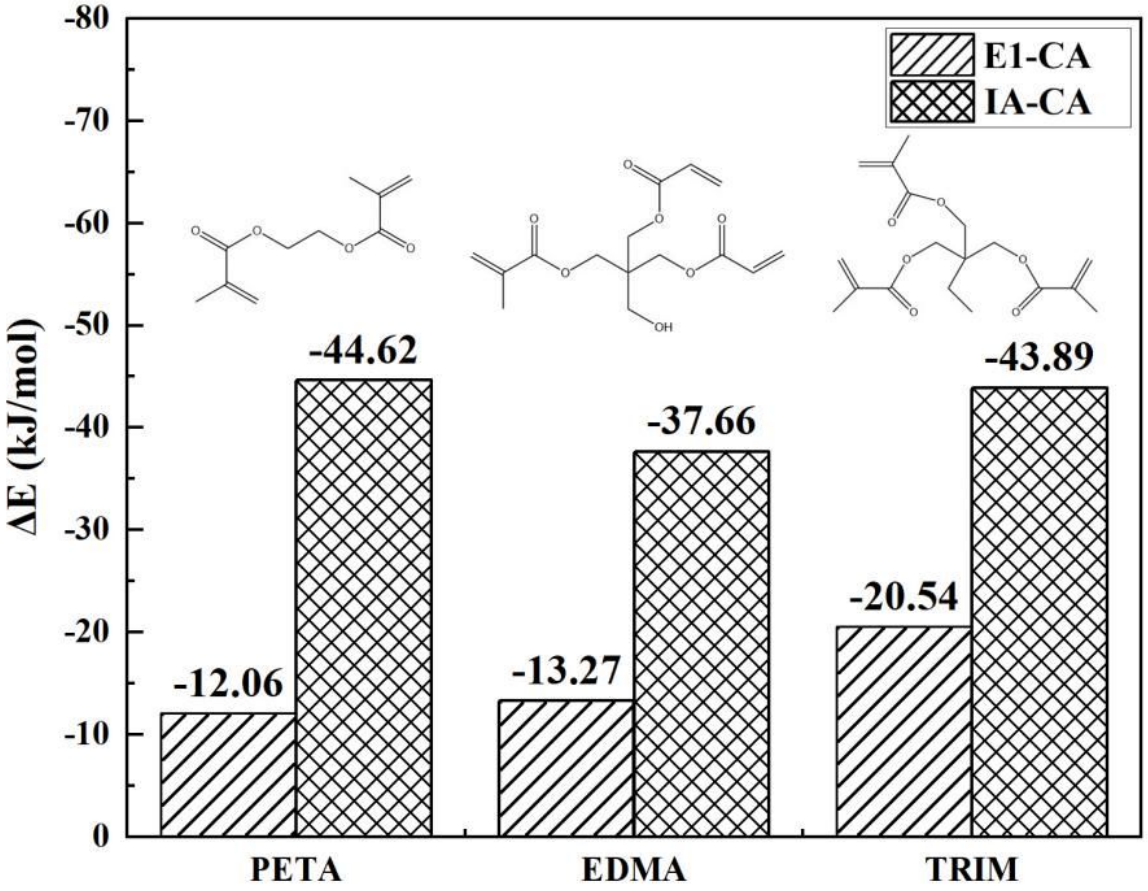

Figure 6

Molecular graphs (a) and contours of Laplacian of electronic density (b) of the complex formed from E1 and IA

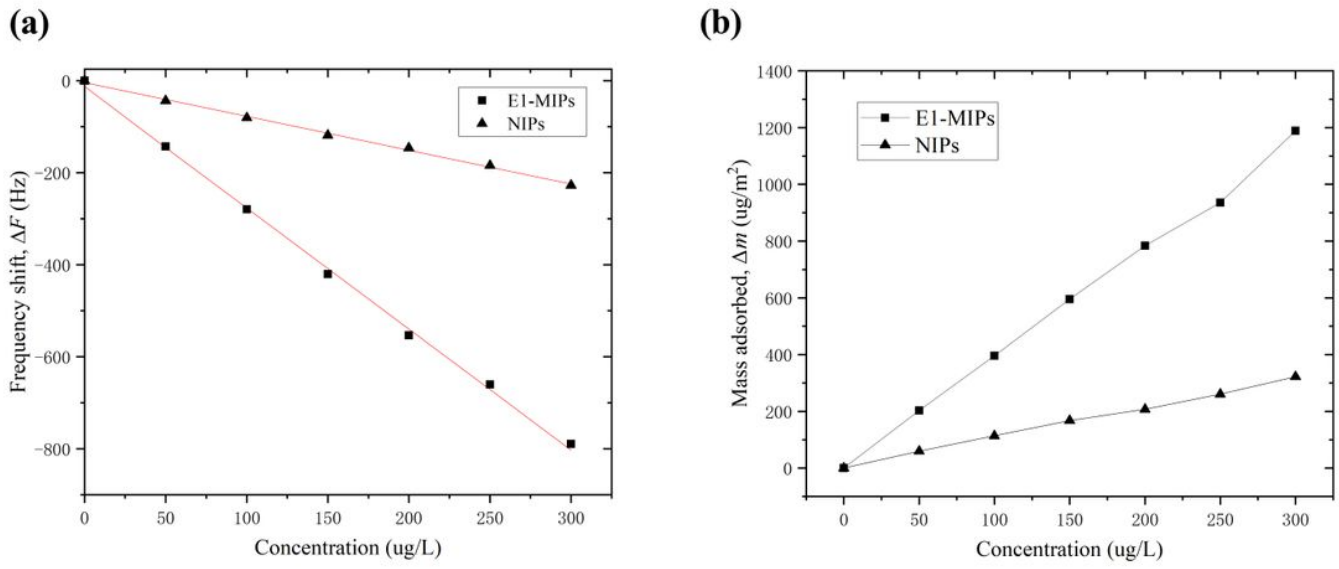

Figure 7

Frequency shift (a) and mass absorbed (b) of the sensor in E1 standard solution with different concentrations

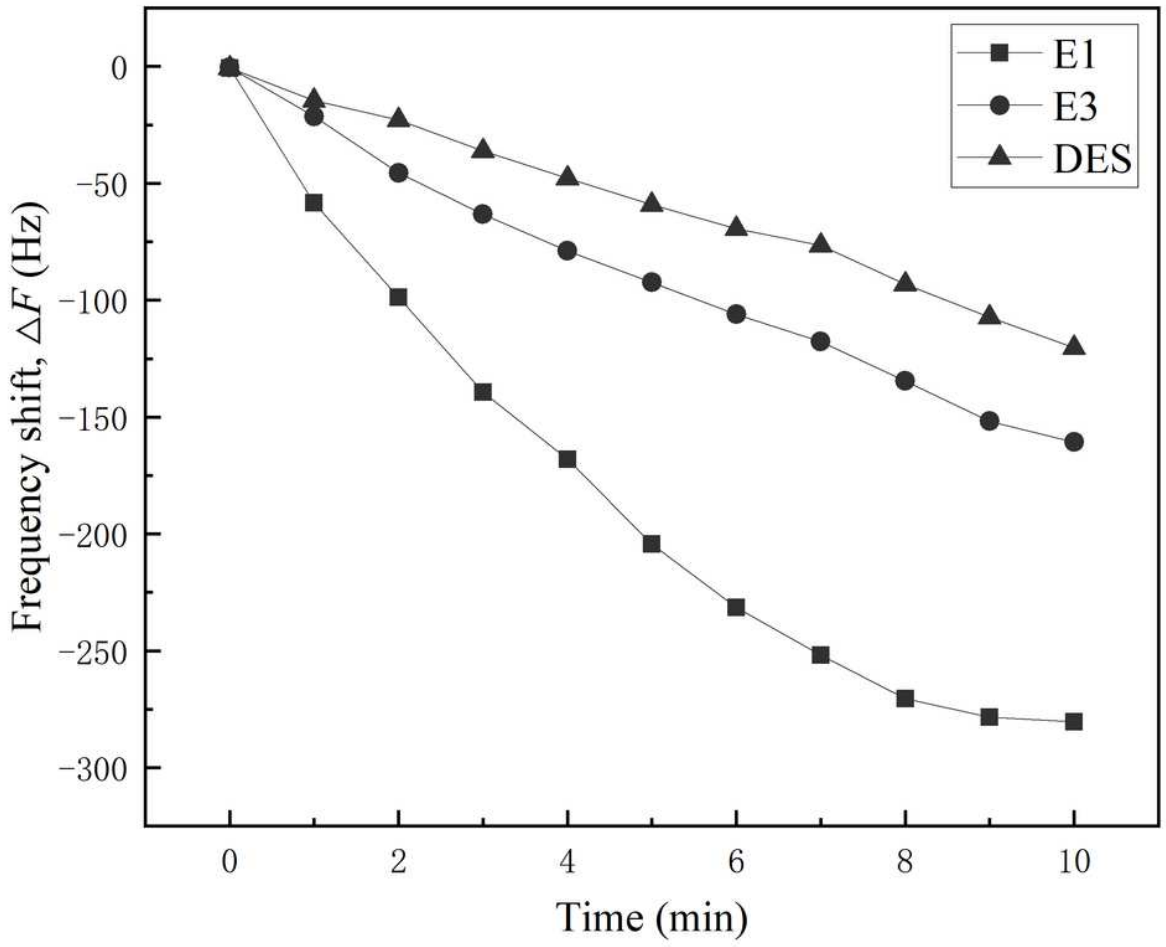

Figure 8

Sensor selectivity of E1, E3, and DES